Univerzita Komenského v Bratislave

Fakulta matematiky, fyziky a informatiky

Michal Broz

Autoreferát dizertačnej práce

BARYON – ANTIBARYON ASYMMETRY IN CENTRAL RAPIDITY REGION AT LHC WITH THE ALICE EXPERIMENT

na získanie akademického titulu philosophiae doctor

v odbore doktorandského štúdia:

4.1.5. jadrová a subjadrová fyzika

Bratislava 30.4.2012

Dizertačná práca bola vypracovaná v dennej forme doktorandského štúdia na Katedre jadrovej fyziky a biofyziky.

Predkladateľ: Mgr. Michal Broz
Katedra jadrovej fyziky a biofyziky
Fakulta matematiky, fyziky a informatiky
Univerzita Komenského
Mlynská Dolina
842 48 Bratislava 4
Slovensko

Školiteľ: prof. RNDr. Branislav Sitár DrSc.

Oponenti: 1.

2.

3.

Obhajoba dizertačnej práce sa koná ..... o ..... h
pred komisiou pre obhajobu dizertačnej práce v odbore doktorandského štúdia vymenovanou predsedom odborovej komisie .....
(uviesť dátum vymenovania)

....
(študijný odbor) (názov študijného programu doktorandského štúdia)

na
.....
(presná adresa miesta konania obhajoby dizertačnej práce)

Predseda odborovej komisie:
.....
(meno a priezvisko s uvedením titulov a hodností
a presná adresa jeho zamestnávateľa)

Contents

Introduction 1

1 Baryon number transport 1

2 Objectives of the thesis 5

3 Results 6

3.1 Data sample 6

3.2 Analysis details 6

3.3 Rapidity and transverse momentum dependence 8

3.3.1 $\boldsymbol{p/p}$ 8

3.3.2 $\boldsymbol{\Lambda/\Lambda}$ 9

3.3.3 $\boldsymbol{\Xi+\Xi-}$ 11

3.3.4 $\boldsymbol{\Omega+\Omega-}$ 12

3.4 Dependence on strangeness and collision energy 12

3.4.1 Central rapidity ratios 12

3.4.2 Rapidity interval and strangeness dependence 13

3.5 Multiplicity dependence 15

3.5.1 $\boldsymbol{p/p}$ 15

3.5.2 $\boldsymbol{\Lambda/\Lambda}$ 16

3.5.3 $\boldsymbol{\Xi+\Xi-}$ 17

3.6 Summary 17

Conclusion 17

References 18

Introduction

It is not obvious which partons in the proton carry its baryon number. In model where the baryon number of the incident baryon is associated with valence quarks and transferred to a more central rapidity region by diquark exchange the mechanism is attenuated exponentially with the rapidity interval over which the baryon charge is moved. Alternatively, when baryon number is carried by gluonic field, baryon number flow can be rapidity independent due to a purely gluonic mechanism. When the baryon number is carried by gluons, there can be nonzero asymmetry in central rapidity. This is accounted for models where the three valence quarks of the proton are fragmented independent but are joined by strings to a baryonic gluon field configuration, the so-called string junction. These two theories can be tested experimentally by measuring the asymmetry of baryon number in central rapidity region.

ALICE has several features that make it an important contributor to proton–proton physics at the LHC. Its design allows particle identification over a broad momentum range, powerful tracking with good resolution from 100 MeV/c to 100 GeV/c, and excellent determination of secondary vertices. These, combined with a low material thickness and a low magnetic field, will provide unique information about low-pt phenomena in pp collisions at the LHC.

1 Baryon number transport

In inelastic non-diffractive proton-proton collision at very high energy, the incoming projectile breaks up into several hadrons that typically emerge, after the collision, at small angles close to the original beam direction. The deceleration of the incoming proton, or more precisely of the conserved baryon number associated with the beam particles, is often called ‘‘baryon-number transport’’ and has been debated theoretically for some time [1], [2], [3-9].

Most of the (anti-) baryons at midrapidity are created in baryon-antibaryon pair production, implying equal yields. Any excess of baryons over antibaryons is therefore associated with the baryon-number transfer from the incoming beam. Note that such

a study has not been carried out in high-energy proton-antiproton colliders (SpS, Tevatron) because of the symmetry of the initial system at midrapidity.

There is a possibility to investigate baryon transport over very large rapidity intervals by measuring the mid-rapidity antibaryon-to-baryon ratio, which can be defined as

$$R_{BN}(y) = \frac{N_{\overline{BN}}}{N_{BN}}. \qquad (1.1)$$

There were several attempts to reproduce the behavior of the experimental results within the framework of different models. Two fundamental models of baryon structure were developed in the past.

The first one "Constituent quark model" [17] introduced the baryon as quark-diquark pair. In this model the valence quarks are carriers of baryon number, each valence quark has BN = 1/3. Gluons are without baryon number. Diquark in this model is a solid structure and can't be divided in the collision. As a consequence the final baryon is produced around this diquark every time, the baryon number is transported in the diquark configuration. This is the only one existing process in composite quark model. Only one string can be broken in this model. However, diquarks in general retain a large fraction of the proton momentum and therefore stay close to beam rapidity, typically within one or two units, as dictated by negative value of α_j for diquark configuration. Therefore, additional processes have been proposed to transport the baryon number over larger distances in rapidity. These processes took place in string junction model.

In the string junction model [1,2], configuration of strings in baryon having minimal energy has a form of the Mercedes - Benz star and the point where the strings joint is called the "string junction". In string junction model, the baryon number is carried by string junction. So for the valence quarks BN = 0 and for the string junction BN = 1. In the string junction model we have a possibility to break one, two or even all the three strings. This leads to two additional processes. The last process when all three string are broken and final baryon is created around string junction with presence of three sea quarks is often called "pure gluonic" process because all the valence quarks were moved away.

The baryon number transport can be described in the framework of Regge phenomenology [16]. In this framework the probability to transfer the baryon number over rapidity interval Δy is [3]

$$\propto \sqrt{s}^{\alpha-1} \approx e^{(\alpha-1)\Delta y} \qquad (1.2)$$

where $\Delta y = y_{beam} - y_{baryon}$ and α is a constant which depends on the configuration in which the baryon number is transported and is identified in the Regge model as the intercept of the trajectory for the corresponding exchange in the *t* channel (see Table 1.1).

	α ≈
Diquark (CQM)	-1/2
SJ accompanied by diquark	-1/2
SJ accompanied by quark [3] [7]	1/2
SJ itself [3] [6]	1/2
SJ itself [4] [5]	1

Table 1.1: α values for different processes in string junction and composite quark model of a baryon. Two values for SJ itslef process coresponds to different teoretical models

At LHC energies we can investigate the convergence of the antibaryon to baryon ratio. Considering the string junction model of the baryon, two marginal values of α_j were debated for pure gluonic process of baryon number transport. These two concepts result in a significantly different BN distribution with rapidity (BN transport), when the proton interacts inelastically at high energies.

- If we take the α_j for pure gluonic process close to 1, then the process is not or just slightly suppressed at large values Δy and as a consequence we can see non-zero asymmetry at 7 TeV. The value equal to unity induce antibaryon-to-baryon ratio converging at high energies to non-unity value.
- Another possibility is that $\alpha_j = 0.5$. This induces vanishing baryon number transport and antibaryon to baryon ratio at 7 TeV close to unity.

A rough approximation of the Δy dependence of the ratio R can be derived in the Regge model, where baryon pair production at very high energy is governed by Pomeron exchange and baryon transport by string-junction exchange [6]. The relevant diagrams that contribute to the production of both antibaryons and baryons are given in Figure1.1.

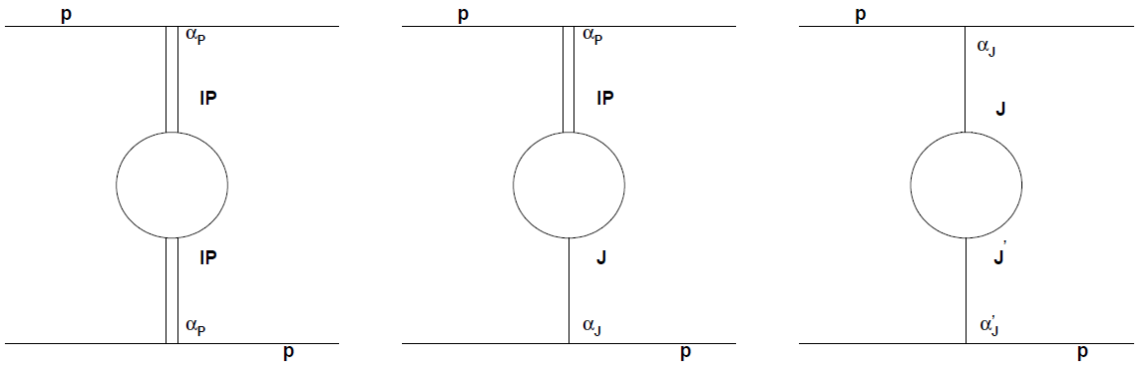

Figure 1.1: Diagrams types contributing to baryon (all) and antibaryon (first one). α values are coresponding to different BN transport processes in string junction or constituent quark model.

Here we consider that pomeron intercept α_p = 1.2 [9] and α_j and α_j‘ are string junction intercepts as summarized in Table 1.1 in all possible combinations.

Antibaryons are coming only from pair production (left diagram on Figure 1.1), therefore:

$$N_{\bar{B}} \approx e^{2(\alpha_p - 1)\Delta y} \qquad (1.3)$$

Baryons are created in pair production too but in addition can be transferred from one or both beams. Therefore:

$$N_B \approx e^{2(\alpha_p - 1)\Delta y} + \sum_i e^{(\alpha_p - 1)\Delta y} . e^{(\alpha_j^i - 1)\Delta y} + \sum_{i,k} e^{(\alpha_j^i - 1)\Delta y} . e^{(\alpha_j^k - 1)\Delta y} \qquad (1.4)$$

Using (1.3) and (1.4) we can derive formula for antibaryon to baryon ratio as a function of rapidity interval Δy

$$1/R = \left(1 + \sum_i C_i e^{(\alpha_j^i - \alpha_p)\Delta y}\right)^2 \qquad (1.5)$$

where *i* = 1, 2 ,3 means string junction accompanied by diquark, quark or flying itself.

More dependencies of the ratio were predicted and can be investigated experimentally

- Strangeness dependence is driven by fact that colliding particles are protons but by string breakage, also strange quarks can be created from the sea and resulting baryon is therefore strange or even multistrange. This fact itself is giving a limitation on amount of baryon number transport for strange particles.

- Transverse momentum can be seen as an indicator of collision hardness. Particles with higher transverse momentum are coming from harder collisions. Harder collisions have in general also higher multiplicity of produced particles, so these two variables: transverse momentum and multiplicity are in some meaning similar. Overall multiplicity coming from event with presence of different baryon number transport process is proportional to number of broken strings. Due to this, in high multiplicity (or high p_t) sample we have higher probability to find events with two or three string breakage. Therefore the overall weights of the processes of BN transport are changing with multiplicity and p_t.
- As was mentioned before, amount of transferred baryon number is decreasing exponentially with Δy. Rapidity dependence of the ratio is direct consequence of this. The further from central region we are, the higher the probability of BN transport is. Due to this the ratio has to decrease as a function of rapidity, if the measured interval around central rapidity is large enough. In ALICE we can see the ratio in central rapidity up to $|y| < 1$ at maximum due to the detector acceptance. We are interested if central region is flat and if we can see any decrease even in this small interval.

2 Objectives of the thesis

Driven by motivations described in previous section this thesis has the following goals: To analyze the antibaryon-to-baryon ratio in the data of proton-proton collisions measured by ALICE experiment at LHC energies $\sqrt{s}$ = 900GeV, 2.76TeV and 7TeV for the baryons – proton, Λ, charged Ξ and charged Ω and find out:

- central rapidity ratio values – the convergence in Δy
- behavior of the ratio in rapidity, transverse momentum and charged particle multiplicity
- possible strangeness dependence

3 Results

3.1 Data sample

The data used for this analysis were collected during the 2010 LHC pp run at collision energy √s = 900 GeV and 7 TeV and in March 2011 at collision energy √s = 2.76 TeV.

900 GeV	2.76 TeV	7 TeV
7M	40M	180M

Table 3.1: Number of analyzed proton-proton events per collision energy

The first step of the analysis is to select a suitable event sample. For the analysis, events were selected based on the online trigger. In addition, at least one of the criteria was requested to be fulfilled as an offline trigger.

Furthermore, in order for the events to be included in the analysis, they should not be flagged as beam-gas by either V0A or V0C.

Events passing both triggers were then selected only if the primary vertex was reconstructed and if the position of the reconstructed vertex diamond was within the selected area.

Total numbers of analyzed events passing these selections are summarized in Table 3.1.

3.2 Analysis details

Antibaryon-to-baryon ratio was analyzed for four baryon species: Proton, Λ, Ξ and Ω. Three of them Λ, Ξ and Ω, called also hyperons are unstable and contains strange quarks. Strange baryons in ALICE are reconstructed using their weak decay topology in charged particles only. Basic characteristics of analyzed baryons are summarized in the Table 3.2.

	Mass(MeV/c^2)	cτ(cm)	Charged decay	B.R.
$p(uud)$	938.27		-	
$\bar{p}(\overline{uud})$				
$\Lambda(uds)$	1115.68	7.89	$\Lambda \to p + \pi^-$	0.64
$\bar{\Lambda}(\overline{uds})$			$\bar{\Lambda} \to \bar{p} + \pi^+$	
$\Xi^-(dss)$	1321.71	4.91	$\Xi^- \to \Lambda + \pi^-$	0.99
$\overline{\Xi^+}(\overline{dss})$			$\overline{\Xi^+} \to \bar{\Lambda} + \pi^+$	
$\Omega^-(sss)$	1672.45	2.46	$\Omega^- \to \Lambda + K^-$	0.68
$\overline{\Omega^+}(\overline{sss})$			$\overline{\Omega^+} \to \bar{\Lambda} + K^+$	

Table 3.2: Main characteristics of the analyzed particles

Raw measurements, which come from the experiment, are distorted by systematical effects. We need to correct our measurements to these effects to see the real physics. As a consequence of symmetries of the experiment, many detector effects such as the acceptance, the reconstruction and the particle identification ones are the same for particles and anti-particles and thus cancel out in the ratio. The systematical effects which do not disappear in ratio, and for which are we going to correct are:

- Absorption
- Contamination by secondary particles (protons, Λ)
- Cut efficiency (protons)

Several quality criteria are defined for the track selection. Each track is required to have been reconstructed in the TPC in the initial outward-in step of tracking and then successfully refitted in the final back-propagation to the primary vertex . It is also required that each track has at least 80 TPC clusters out of a maximum of 159.

In antiproton-to-proton analysis to reduce the contamination from background tracks (i.e. originating from the interaction of a particle with the material), the selected tracks were required to have at least two associated ITS clusters. Furthermore, a track must have at least one associated ITS cluster on either of the SPD layers. To further reduce the contamination from background and secondary tracks (i.e. (anti)protons originating from the weak decay of Λ), a cut on the distance of closest approach in xy plane (dca_{xy}) of the track to the primary vertex was set.

The Λ, Ξ and Ω are identified by applying selections on the characteristics of their daughter tracks and using their weak decay topologies in the channels listed in Table 3.1.

The momentum as well as the particle identification (PID) relied for this analysis on the information from the TPC detector. The *dE/dx* resolution of the TPC is 5% and depends slightly on number of TPC clusters and inclination angle. To ensure the best identification efficiency and the lowest possible contamination, the minimum number of TPC clusters used for the energy loss calculation was set to 80.

The (anti)protons were selected by defining a band with a 3σ width with respect to teoretical Bethe-Bloch parametrization.

For Λ, Ξ and Ω the particle identification of daughter tracks helps substantialy to decrease the background, especialy in the low p_t – high $|y|$ areas. The selection here concerns all daughters.

Additional cuts are used in case of Λ and Ω. We are excluding the candidates falling into 10 MeV mass window around K^0_s or Ξ nominal mass.h

3.3 Rapidity and transverse momentum dependence

3.3.1 $\bar{p}/p$

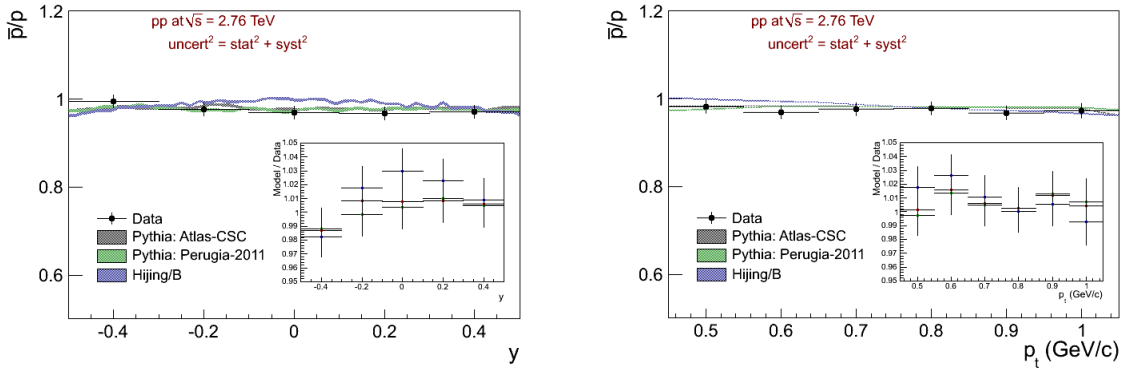

Figure 3.1: $\bar{p}/p$ ratio as function of rapidity and transverse momentum at $\sqrt{s}$ = 2.76 TeV. Data points are compared with different monte carlo predictions. Inset is showing model over data ratios.

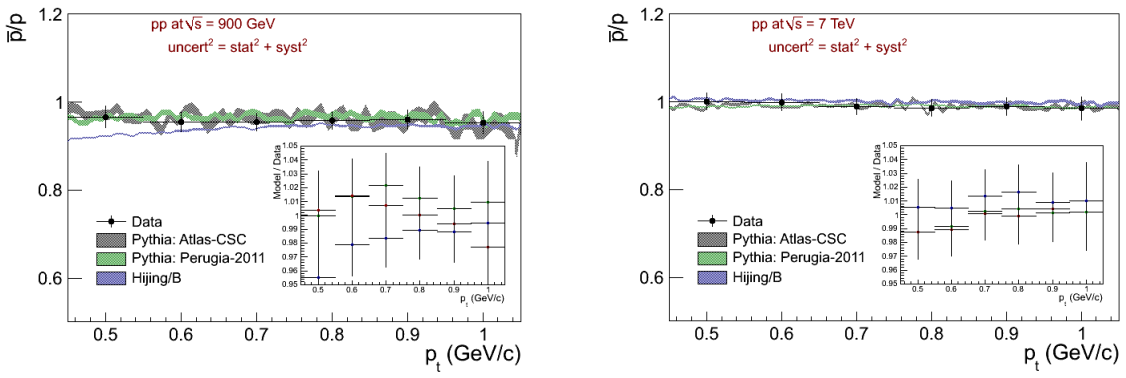

Figure 3.2: $\bar{p}/p$ ratio as function of transverse momentum at $\sqrt{s}$ = 0.9 and 7 TeV. Data points are compared with different monte carlo predictions. Inset is showing model over data ratios.

For $\bar{p}/p$ ratio we dont see any sign of rapidity or transverse momentum depenedence. Data points are well described by PYTHA tunes: Atlas-CSC and Perugia-2011 and by HIJING/B.

3.3.2 $\bar{\Lambda}/\Lambda$

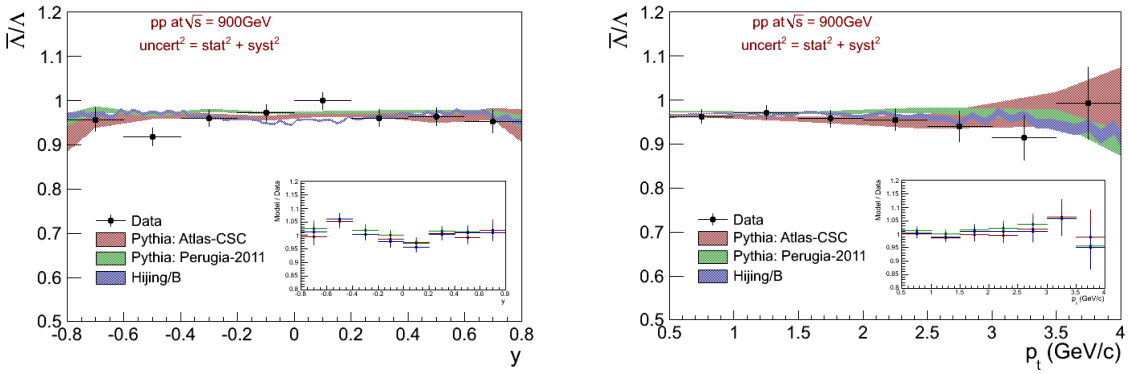

Figure 3.3: $\bar{\Lambda}/\Lambda$ ratio as function of rapidity and transverse momentum at $\sqrt{s}$ = 900 GeV. Data points are compared with different monte carlo predictions. Inset is showing model over data ratios.

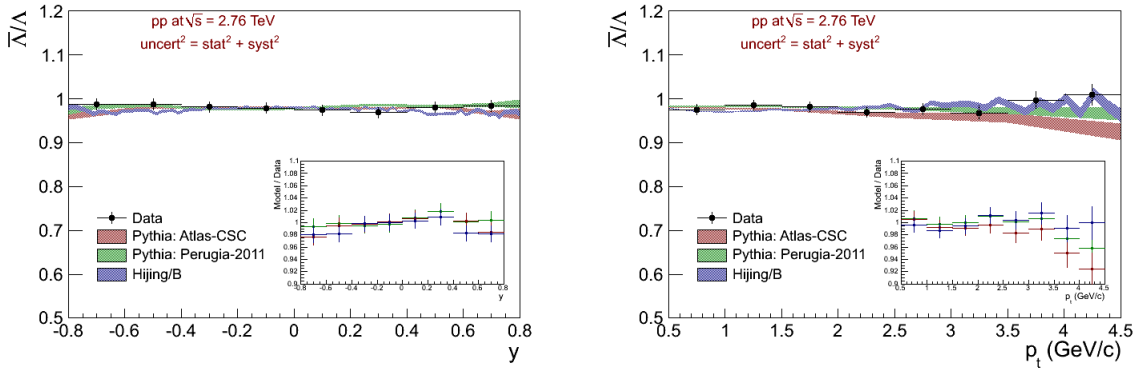

Figure 3.4: $\bar{\Lambda}/\Lambda$ ratio as function of rapidity and transverse momentum at $\sqrt{s} = 2.76$ TeV. Data points are compared with different monte carlo predictions. Inset is showing model over data ratios.

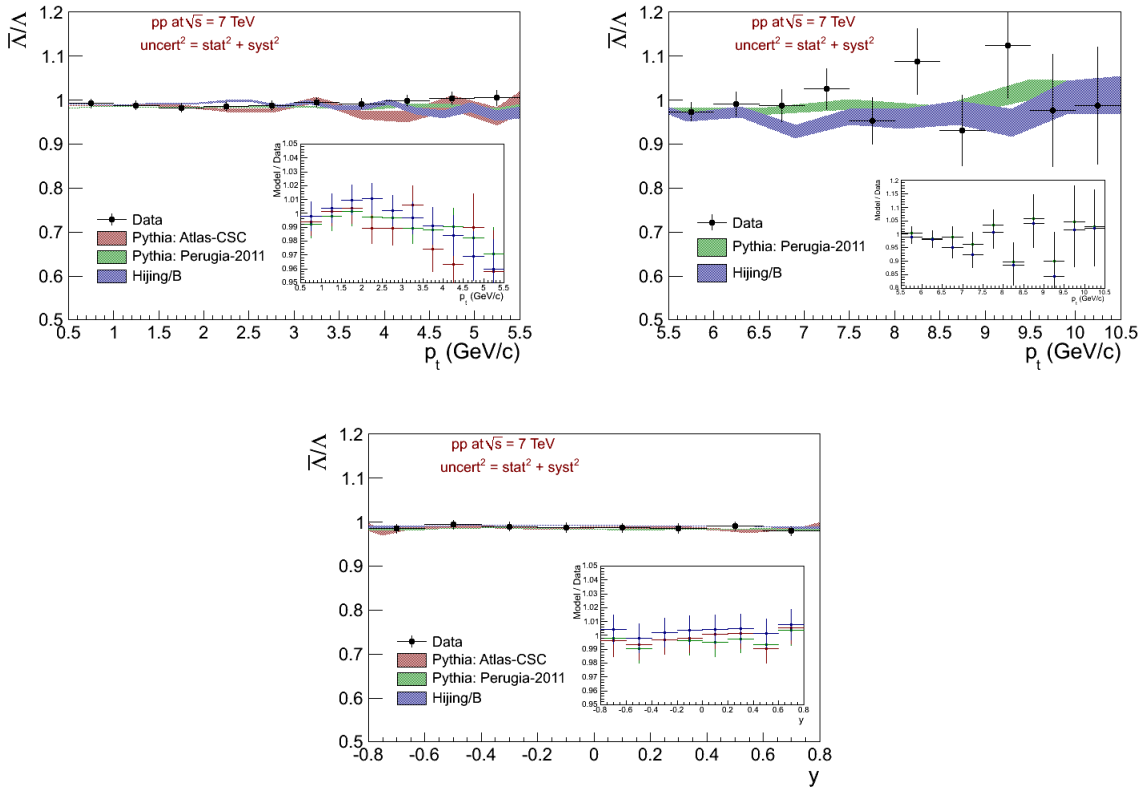

Figure 3.5: $\bar{\Lambda}/\Lambda$ ratio as function of rapidity and transverse momentum at $\sqrt{s} = 7$ TeV. Data points are compared with different monte carlo predictions. Inset is showing model over data ratios..

For $\bar{\Lambda}/\Lambda$ ratio we dont see any sign of rapidity or transverse momentum depenedence. Data points are well described by PYTHA tunes: Atlas-CSC and Perugia-2011 and by HIJING/B.

At √s = 7TeV two phase space regions were analyzed separatelly. The first one in low p_t up to 5.5 GeV/c was analyzed in two dimensions using all corrections described in section 3.2. The second one in p_t higher then 5.5 GeV/c was analyzed in transverse momentum only and on top of that, no correction were applied. This was induced by fact that all the corrected effect vanish, and are negligible in this region. Mid rapidity ratios in both regions are compatible (see Table 3.3)

$0.5 < p_t$ (GeV/c) < 5.5	$5.5 < p_t$ (GeV/c) < 10.5
0.989±0.001±0.010	0.986±0.013±0.008

Table 3.3: Mid-rapidity $\bar{\Lambda}/\Lambda$ ratio at $\sqrt{s}$ = 7 TeV in different p_t areas. Values are printed with statistical and systematical uncertainity

3.3.3 $\overline{\Xi^+}/\Xi^-$

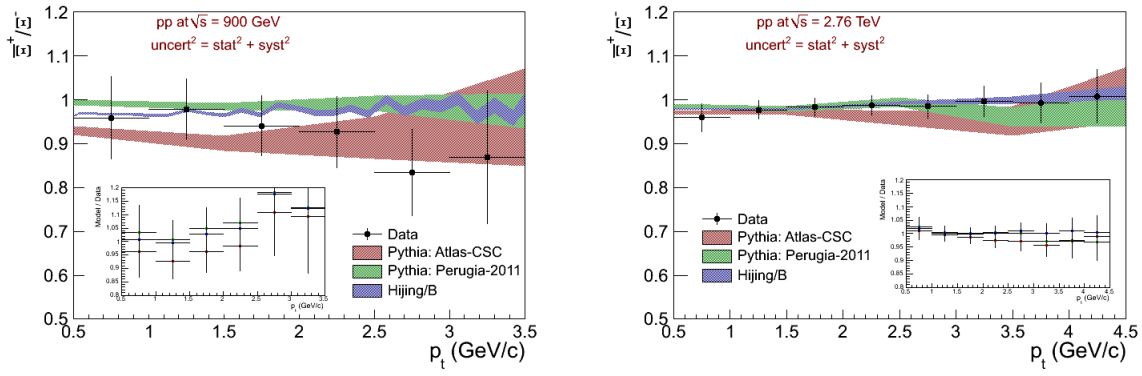

Figure 3.6: $\overline{\Xi^+}/\Xi^-$ ratio as function of transverse momentum at √s = 0.9 and 2.76 TeV. Data points are compared with different monte carlo predictions. Inset is showing model over data ratios.

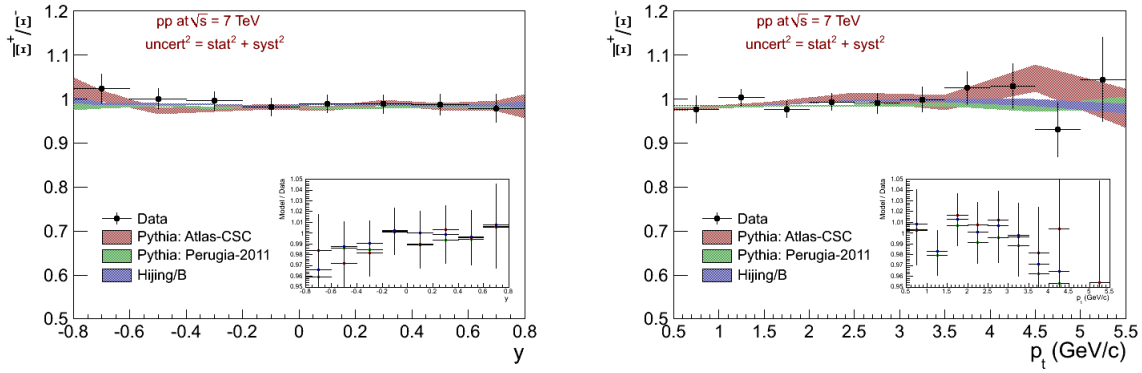

Figure 3.7: $\overline{\Xi^+}/\Xi^-$ ratio as function of rapidity and transverse momentum at √s = 7 TeV. Data points are compared with different monte carlo predictions. Inset is showing model over data ratios.

For $\overline{\Xi^+}/\Xi^-$ratio we dont see any sign of rapidity or transverse momentum depenedence. Data points are well described by PYTHA tunes: Atlas-CSC and Perugia-2011 and by HIJING/B.

3.3.4 $\overline{\Omega^+}/\Omega^-$

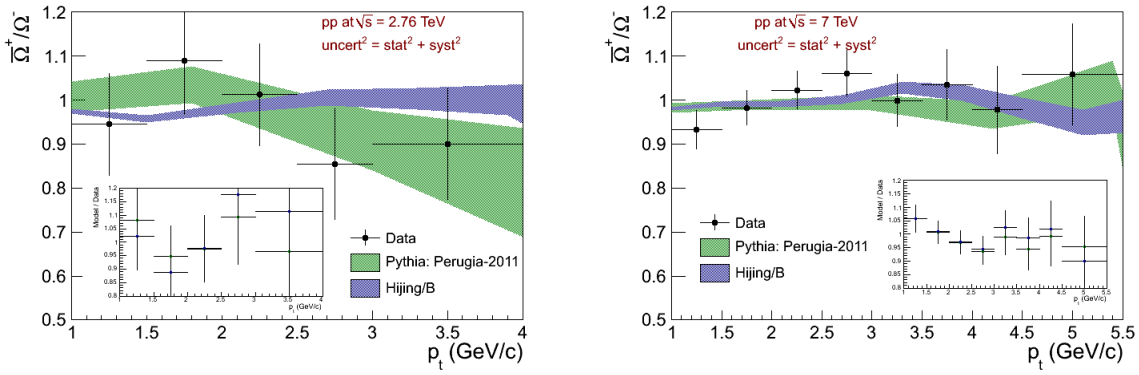

Figure 3.8: $\overline{\Omega^+}/\Omega^-$ratio as function of transverse momentum at √s = 2.76 and 7 TeV. Data points are compared with various monte carlo predictions. Inset is showing model over data ratios.

For $\overline{\Omega^+}/\Omega^-$ratio we dont see any sign of transverse momentum depenedence. Data points are well described by PYTHA tunes: Atlas-CSC and Perugia2011 and by HIJING/B.

3.4 Dependence on strangeness and collision energy

3.4.1 Central rapidity ratios

Final corrected antibaryon-to-baryon ratio integrated within our rapidity and transverse momentum acceptance for different particle species and √s is summarized in Table 3.4 and Figure 3.9.

	P	**Λ**	**Ξ**	**Ω**
900 GeV	0.957±0.006±0.014	0.963±0.006±0.012	0.938±0.028±0.044	No statistics
2.76 TeV	0.975±0.004±0.014	0.979±0.002±0.011	0.982±0.008±0.014	0.964±0.05±0.043
7 TeV	0.991±0.005±0.014	0.989±0.001±0.010	0.992±0.006±0.012	0.997±0.016±0.02

Table 3.4: Central rapidity ratios. Values are integrated in $|y| < 0.5$ for $\bar{p}/p$ and in $|y| < 0.8$ for the rest. Uncertainities corresponds to statistical and systematical ones.

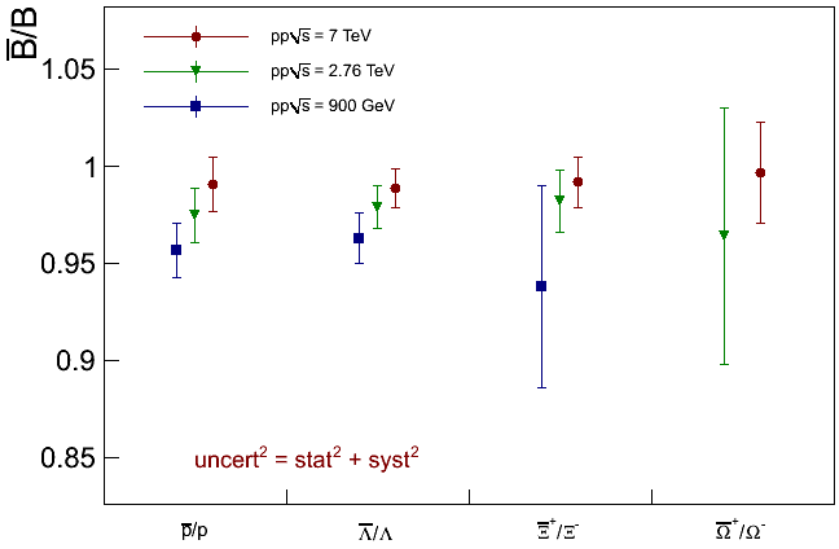

Figure 3.9: Central rapidity ratios. Values are integrated in $|y| < 0.5$ for $\bar{p}/p$ and in $|y| < 0.8$ for the rest.

At 900 GeV and 2.76 TeV we can still see a small excess of baryons over antibaryons for protons, Λ and Ξ (only 2.76 TeV), but at 7 TeV the ratio is compatible with unity for all measured baryons. The ratios at 0.9 and 7 TeV are significantly different for protons Λ and Ξ since the systematic uncertainitites are fully correlated. The fact that ratio at 7 TeV is compatible with unity sets an stringent limit on amouth of transported baryon number over 9 units in rapidity. The existence of large values of antibaryon-to-baryon asymmetry even at infinite energy (A = 0.035 [11]), as was predicted by models using α = 1 for pure gluonic process of baryon number transfer is therefore excluded.

3.4.2 Rapidity interval and strangeness dependence

We can parametrize the rapidity interval dependence of $\bar{p}/p$, $\bar{\Lambda}/\Lambda$ and $\overline{\Xi^+}/\Xi^-$ ratio with presence of our points and previous experimental measurements in proton-proton collisions [11-15] using function (1.5) The constants that are adjusted to experimental points using pomeron intercept $\alpha_p = 1.2$ and junction intercepts as summarized in the Table 1.1 are summarized in the Table 3.5 and Table 3.6.

	Diquark-SJ(-1/2)	Quark-SJ(1/2)	SJ itself(1)
$\bar{p}/p$	81 ± 10	3.35 ± 0.52	0.01 ± 0.03
$\bar{\Lambda}/\Lambda$	50 ± 7	1.78 ± 0.28	0.01 ± 0.02
$\overline{\Xi^+}/\Xi^-$	0(set)	1.97 ± 1.8	0.007 ± 0.05

Table 3.5: Results of parametrization using function (1.5). Constants are corresponding to processes with different junction intercept (value in the bracket) according to configuration in which the baryon number is transported.

	$C(\alpha_J=1/2)$
$\bar{p}/p$	9.91 ± 0.92
$\bar{\Lambda}/\Lambda$	5.20 ± 0.43
$\overline{\Xi^+}/\Xi^-$	4.52 ± 2.28

Table 3.6: Results of parametrization using function (1.7)

As was said already in previous section, the ratio is convergating to unity - is at 7 TeV compatible with unity for all baryon species. This leads to negligibility of the process using $\alpha = 1$ as can be seen on Table 4.10.

We can conclude that

- the process with $\alpha_J = 1$ doesnt improve the quality of the fit, and its contribution is compatible with zero.
- results are consistent with predictions using $\alpha_J = 0.5$ for string junction – itlself configuration
- any significant contribution to antibaryon-to-baryon ratio at central rapidity due to an exchange which is not suppressed with increasing rapidity interval is disfavored
- the process with $\alpha_J = -1/2$ included in parameterization (1.5) does improve the fit at low values of Δy (~3)

We can draw all the parameterizations onto one plot and we can see that it describes also strangeness dependence well. At least for $\bar{p}/p$ and $\bar{\Lambda}/\Lambda$ the functions are well separated. Due to large uncertainity of the paramaterizations of $\overline{\Xi^+}/\Xi^-$ and $\overline{\Omega^+}/\Omega^-$ ratio we cant make any conclusion for multistrange baryons.

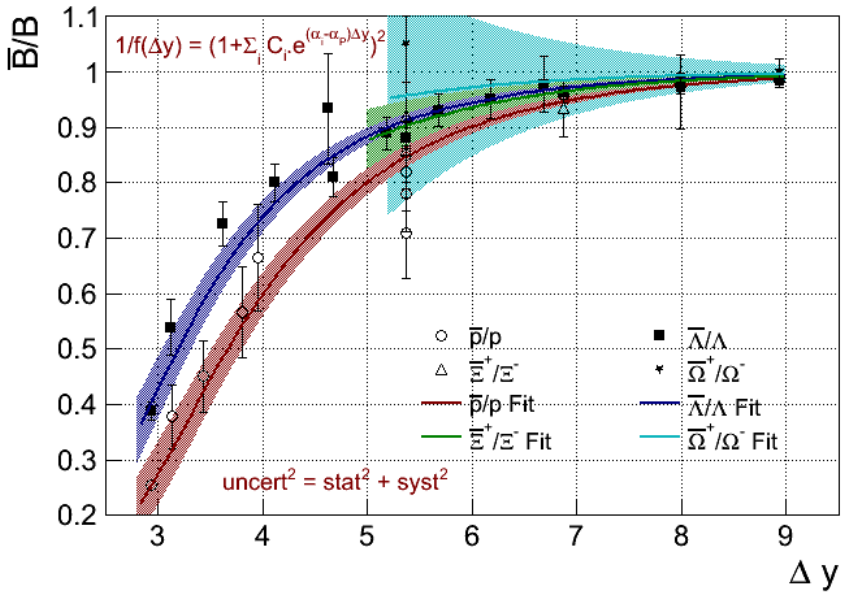

Figure 3.10: Central rapidity ratio as a function of rapidity interval for measured baryons. Parametrization with function (1.5) is showed. Shaded areas around the functions correspond to uncertainity of the function coming from uncertainity of adjusted parameters.

3.5 Multiplicity dependence

Charged particle multiplicity estimator for this measurement is based on the number of ITS standalone tracks + number of tracklets (vectors connecting pair of SPD1 and SPD2 clusters and pointing to vertex within some angular tolerance) for the particles not reconstructed as a full track.

Distribution is divided into multiplicity bins with respect to reasonable statistics in each bin. The weighted mean and standard deviation σ of the multiplicity distribution in the bin range was set as center and x error bar of a point in multiplicity dependence of the ratio.

3.5.1 $\bar{p}/p$

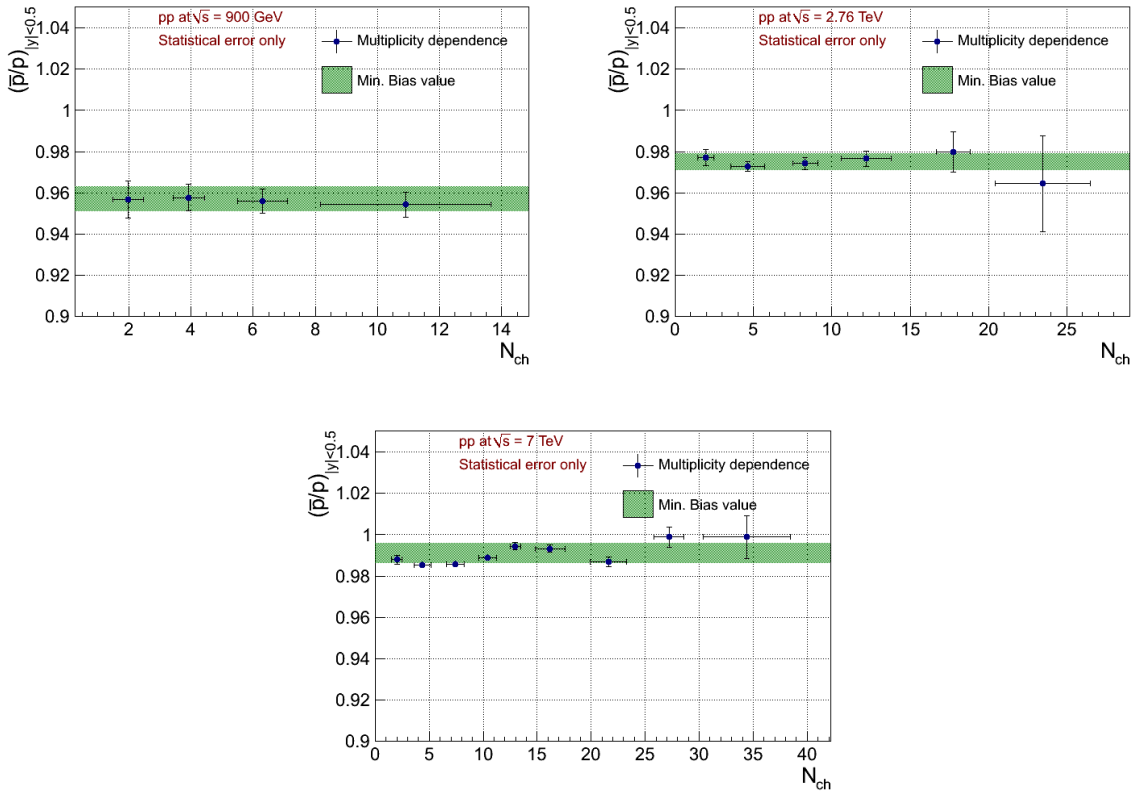

Figure 3.11: $\bar{p}/p$ ratio as function of charged particle multiplicity at √s = 0.9, 2.76 and 7 TeV. The ratio is calculated for the interval |y| < 0.5. The error bars corresponds to statistical ones.

The $\bar{p}/p$ ratio is not showing any sign of charged multiplicity depenedence.

3.5.2 $\bar{\Lambda}/\Lambda$

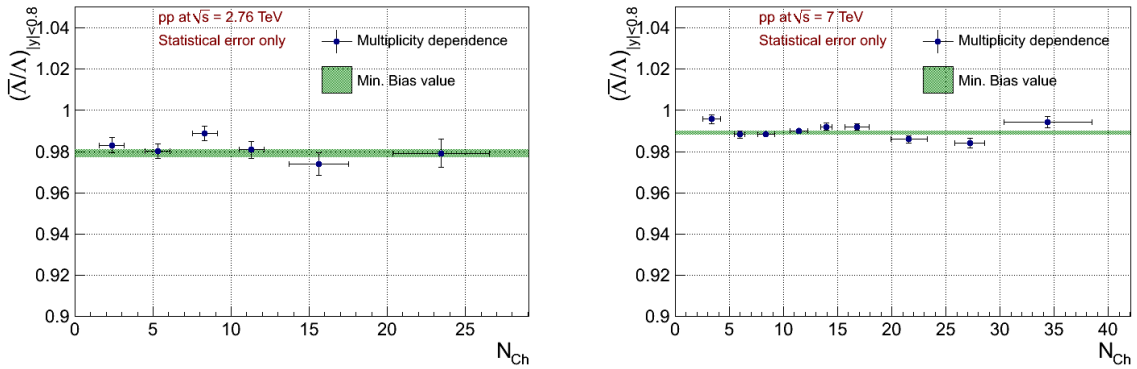

Figure 3.12: $\bar{\Lambda}/\Lambda$ ratio as function of charged particle multiplicity at √s = 2.76 and 7 TeV. The ratio is calculated for the interval |y| < 0.8. The error bars corresponds to statistical ones.

The $\bar{\Lambda}/\Lambda$ ratio is not showing any sign of charged multiplicity depenedence.

3.5.3 $\overline{\Xi^+}/\Xi^-$

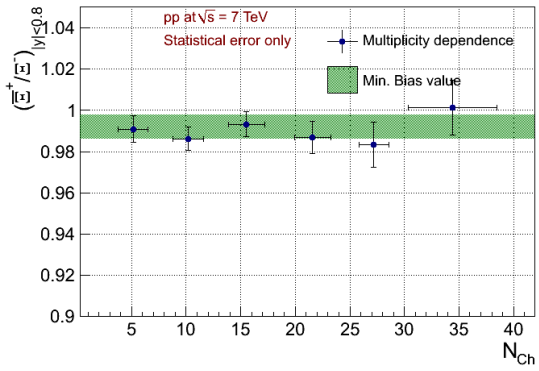

Figure 3.13: $\overline{\Xi^+}/\Xi^-$ ratio as function of charged particle multiplicity at √s = 7 TeV. The ratio is calculated for the interval |y| < 0.8. The error bars corresponds to statistical ones.

The $\overline{\Xi^+}/\Xi^-$ ratio is not showing any sign of charged multiplicity depenedence.

3.6 Summary

In summary we report the ratio of the midrapidity anti-baryon to baryon yield for proton, Λ, charged Ξ and charged Ω baryons in proton-proton collisions a √s = 0.9, 2.76 and 7 TeV. Within the fiducial acceptance region (see Table 3.7) the ratio is found to be very close to unity and independent of both rapidity and transverse momentum (see Figure 3.1 – 3.8). We don't see any sign of charged multiplicity dependence too (see Figure 3.12 – 3.14).

	√s (TeV)	**p**	**Λ**	**Ξ**	**Ω**
y	0.9 – 2.76 – 7	0.5		0.8	
p_t (GeV/c)	0.9	0.45 – 1.05	0.5-4.0	0.5-3.5	-
	2.76		0.5-4.5	0.5-4.5	1.0-4.0
	7		0.5-10.5	0.5-5.5	1.0-5.5

Table 3.7: Fiducial acceptance region

At 900 GeV we still see small excess of baryons over antibaryons for protons, Λ and Ξ. At 2.76 TeV the excess is even smaller and significant only for protons and Λ. At 7

TeV ratio is compatible with unity for all analyzed baryon species (see Figure 3.9 and Table 3.4). Antibaryon – to baryon ratio is rising with collision energy and converging to unity at 7 TeV for all baryon species (see Figure 3.11). Results are consistent with model predictions using for the baryon-number transport a t-channel exchange with the Regge-trajectory intercept of $\alpha_J \approx 0.5$. Any significant contribution to baryon–antibaryon asymmetry at central rapidity due to an exchange, which is not suppressed with increasing rapidity interval ($\alpha_J \approx 1$), is disfavored. In another words results are consistent with standard models ($\alpha_J \approx 0.5$) of baryon-number transport and set tight limits on any additional contributions to baryon-number transfer over very large rapidity intervals in proton – proton collisions.

Conclusion

I analyzed the data of proton-proton collisions at three LHC energies $\sqrt{s}$ = 900 GeV, 2.76 and 7 TeV. In particular the rapidity, transverse momentum and charged particle multiplicity dependencies of antibaryon-to-baryon ratio are presented. On the top of this, strangeness and rapidity interval dependence of the central rapidity ratio was investigated. Data points were compared with several Monte Carlo predictions. Central rapidity ratios, with participation of previous experimental results were parameterized as a function of rapidity interval and strangeness using function derived in chapter 1. Using the parameterization derived in this thesis I can properly describe rapidity interval dependence and partially describe strangeness dependence of central rapidity ratio.

The main conclusions implied by results of this thesis are:

- Within the fiducial acceptance region (see Table 3.7) the $\bar{p}/p$, $\overline{\Lambda}/\Lambda$, $\overline{\Xi^+}/\Xi^-$ and $\overline{\Omega^+}/\Omega^-$ ratio is found to be very close to unity and independent of rapidity, transverse momentum (see Figure 3.1 – 3.8) and charged particle multiplicity (see Figure 3.12 – 3.14).
- At $\sqrt{s}$ = 900 GeV we see small excess of baryons over antibaryons for protons, Λ and charged Ξ. At $\sqrt{s}$ = 2.76 TeV we still see small excess of baryons over antibaryons for protons and Λ. At 7 TeV ratio is compatible with unity for all analyzed baryon species (see Figure 3.9 and Table 3.4).

- Antibaryon – to baryon ratio is rising with collision energy and converging to unity at 7 TeV for all baryon species (see Figure 3.11).
- Any significant contribution to baryon-antibaryon asymmetry at central rapidity due to an exchange, which is not suppressed with increasing rapidity interval ($\alpha_J \approx 1$), is disfavored.
- Results are consistent with standard models of baryon-number transport ($\alpha_J \approx 0.5$) and set tight limits on any additional contributions to baryon-number transfer over very large rapidity intervals in proton – proton collisions.
- Rapidity interval dependence of antibaryon-to-baryon ratio can be well described by Regge model inspired parameterizations (1.5) in whole Δy range (see Figure 3.11).
- Strangeness dependence of the ratio can be partially described (with respect to the uncertainties) by Regge model inspired parameterization (1.5) of baryon-antibaryon asymmetry (see Figure 3.11).

Preliminary results of the analysis were presented on several international conferences and published in the conference proceedings. Notably I presented the preliminary results on conference "Physics at LHC (PLHC)" 2010 in Hamburg and 2011 in Perugia. Part of the results, transverse momentum dependence of the $\bar{p}/p$ ratio at $\sqrt{s} = 900$ GeV and 7 TeV and parameterization of rapidity interval dependence of $\bar{p}/p$ ratio, was published in Physics Review Letters [10]. In the present time we are working on publication dedicated to the rest of the results showed in this thesis.

References

[1] M. Imachi, S.Otsuki, and F. Toyoda, Prog. Theor. Phys. **52**, 341 (1974)

[2] X. Artru, Nucl. Phys. **B85** (1975) 442

[3] G. C. Rossi and G. Veneziano, Nucl. Phys. **B123**, 507 (1977).

[4] B. Z. Kopeliovich, Sov. J. Nucl. Phys. **45**, 1078 (1987);

[5] B. Z. Kopeliovich and B. Povh, Z. Phys. **C 75**, 693 (1997);
Phys. Lett. **B 446**, 321 (1999).

[6] D. Kharzeev, Phys. Lett. **B 378**, 238 (1996).

[7] C. Merino et al., Eur. Phys. J. **C 54**, 577 (2008);

C.Merino, M. M. Ryzhinskiy, and Yu. M. Shabelski, arXiv:0906.2659.

[8] S. E. Vance and M. Gyulassy, Phys. Rev. Lett. **83**, 1735 (1999).

[9] A. B. Kaidalov, L. A. Ponomarev, and K. A. Ter-Martirosyan, Sov. J. Nucl. Phys. **44**, 468 (1986).

[10] ALICE collaboration: Phys. Rev. Lett. **105**, 072002 (2010

[11] T. Anticic et al. (NA49 Collaboration), Eur. Phys. J. C **65**, 9 (2010).
T. Susa et al. (NA49 Collaboration), Nucl.Phys. A**698** (2002) 491-494

[12] A. M. Rossi et al., Nucl. Phys. **B84**, 269 (1975);
M.Aguilar-Benitez et al., Z. Phys. **C 50**, 405 (1991).

[13] B. I. Abelev et al. (STAR Collaboration), Phys. Rev. **C 79**, 034909 (2009);
I.G. Bearden et al. (BRAHMS Collaboration), Phys. Lett. **B 607**, 42 (2005); B.B. Back et al. (PHOBOS Collaboration), Phys. Rev. **C 71**, 021901 (2005);
S. S. Adler et al. (PHENIX Collaboration), Phys. Rev. **C 69**, 034909 (2004).

[14] B. I. Abelev et al. (STAR Collaboration), Phys. Rev. C **75** (2007) 64901

[15] LHCb collaboration: JHEP08(2011)034

[16] P. D. B. Collins, An Introduction to Regge Theory and High Energy Physics (Cambridge University Press, Cambridge, England, 1977).

[17] D. B. Lichtenberg and L. J. Tassie, Phys. Rev. 155, 1601 (1967)

Publications

[I] Michal Broz for the ALICE Collaboration: [PLHC 2010 proceedings] Baryon-antibaryon asymmetry in the central rapidity region at √s = 0.9 TeV and 7 TeV with ALICE; DESY-PROC-2010-01/276

[II] Michal Broz for the ALICE Collaboration: [PLHC 2011 proceedings] Baryon number transport at LHC energies with the ALICE experiment;

[III] ALICE Collaboration: Strange particle production in proton-proton collisions at √s=0.9 TeV with ALICE at the LHC; Eur. Phys. J. C**71** (2011): 1594

[IV] ALICE Collaboration: Production of pions, kaons and protons in pp collisions at √s = 900 GeV with ALICE at the LHC; Eur.Phys.J. C**71** (2011): 1655

[V] ALICE Collaboration: Multi-strange baryon production in pp collisions at √s = 7 TeV with ALICE; arXiv:1204.0282 [nucl-ex]